En-route Flight Trajectory Prediction for Conflict Avoidance and Traffic Management

G. B. Chatterji*, B. Sridhar†, and K. D. Bilimoria‡
NASA Ames Research Center
Moffett Field, CA 94035

Abstract

Great circle flight during the en-route phase is examined with the goal of trajectory prediction. Equation of the great circle is used for deriving closed form solutions of the course angle required for flying the great circle. The heading angle required for flying the course angle in the presence of winds aloft is described. Since aircraft maintain airspeed or Mach number rather than groundspeed, the location of the aircraft cannot be precisely predicted sometime into the future without adequate knowledge of the wind and temperature. A wind forecast model that provides the wind and temperature data is described. Since groundspeed depends on temperature, windspeed and track-relative wind heading, equations that describe its sensitivity with respect to these variables are presented. An algorithm is presented for predicting the nominal trajectory based on the data derived from the forecast model. Finally, an algorithm for estimating error bounds around the nominal trajectory is presented. The error bounds are determined by propagating the wind forecasting errors along the nominal trajectory.

1 Introduction

Under the current air traffic rules airplanes are required to follow designated routes, which in the United States are referred to as *victor airways* and *jet routes*. The route system consists of a network of navigational aids and air traffic control facilities for providing safe and orderly flow of traffic. Airplanes are required to comply with the minimum separation rules in the vertical, longitudinal and lateral directions [1]. Minimum separation rules are a function of aircraft type, speed, availability of tracking facilities and additional factors such as wake vortices. Lateral separation is established by route structures with protected airspace that does not overlap to keep aircraft at a particular altitude on different routes. Vertical separation is established by assigning 1000 feet between aircraft up to and including 29,000 feet altitude. Above 29,000 feet, a separation of 2000 feet is required. When the aircraft mix is such that wake turbulence is not a factor and sensor coverage is available, the minimum longitudinal separation for two aircraft at the same altitude is five nautical miles. A reduced separation of three miles may be used when the aircraft are within 40 nautical miles from the radar antenna. Speed control is the primary mechanism for maintaining longitudinal separation.

The current air traffic route structure is capacity and flexibility limited [2]. It has been argued that recent and future technological enhancements in the areas of communication, navigation and surveillance have the potential for automation in the cockpit and on the ground for conflict identification and elimination. The goal is to provide aviation users the flexibility of Visual Flight Rules (VFR) while maintaining the protection available under the Instrument Flight Rules (IFR). Free flight is envisioned to accomplish this goal. The Radio Technical Commission for Aeronautics (RTCA) defines free flight as a safe and efficient flight operating capability under IFR in which the operators have the freedom to select their path and speed in real time. Air traffic restrictions are imposed only to ensure separation, to preclude exceeding airport capacity, to prevent unauthorized flight through special use airspace, and to ensure safety of flight. Restrictions are limited in extent and duration to correct the identified problem [2]. The impact of free flight is largely associated with the en-route portion of the flight which begins 200 miles beyond the departure airport and ends 200 miles before the arrival airport. This motivates the current study of the en-route phase of flight.

During the en-route phase of the flight user preferred routing will be permitted. This means that aircraft will be able to take advantage of the on-board systems to fly optimum flight paths. Current generation Flight Management Systems (FMS) are capable of flying optimal trajectories for input cost index. This index is a function of current fuel prices and crew costs. The FMS constructs both lateral and vertical paths based on predicted winds, selected cruise speed and airplane

*Research Specialist, Sterling Federal Systems Group; MS 262-6.
†Chief, AFF Branch; MS 262-3. Associate Fellow AIAA.
‡Research Specialist, Sterling Federal Systems Group; MS 262-6. Associate Fellow AIAA.

performance model, as described in [3]. Since airplane performance parameters are closely tied to the Mach number, it is directly controlled by the FMS. However, groundspeed rather than airspeed resulting from the Mach number, is needed for locating the airplane in an earth fixed coordinate frame. To be able to determine the groundspeed, the windspeed and direction are required in addition to the airspeed. Without an adequate knowledge of groundspeed, separations required for air traffic control in a free flight environment cannot be guaranteed. Trajectory prediction, which is based on groundspeed, is the key to conflict detection and maintainance of separation minimums. In this research, great circle en-route flight is examined with the goal of trajectory prediction.

Subsequent sections are organized as follows. Great circle equation is derived in Section 2. Kinematic equations are used along with great circle equation to derive closed-form solutions of the course angle required to fly the great circle route in Section 3. The heading angle required for maintaining the desired course angle in the presence of winds is also described in Section 3. Since trajectory prediction requires groundspeed which in turn depends on temperature and winds, the sensitivity of groundspeed is explored in Section 4 with the purpose of developing error models for position uncertainty prediction. The error models are used in Section 5 for position uncertainty prediction. Two algorithms, one for prediction of the nominal trajectory and the other for prescribing uncertainty bounds on the nominal trajectory, are also described in Section 5. The position uncertainty bounds are compared with 5000 Monte Carlo simulations in Section 6. The paper is concluded in Section 7. Finally, a weather forecasting model is described in Appendix A.

2 Great Circle

Great circle is the shortest length curve between two points on a sphere. This problem is also referred to as the geodesics problem in literature. It is known that this curve is the intersection of the sphere with the plane passing through the center of the sphere and the two points on the sphere. This fact can be derived using the calculus of variations approach as shown in [4].

Let a frame of reference be defined as follows. Earth-centered right-handed Cartesian coordinate system with the z-axis in the direction of the north pole and x-axis in the direction of the intersection of the equator and prime meridian. It is noted that the origin in this case is at $(0,0,0)$. Let (x_i, y_i, z_i) be the coordinates of the departure point and (x_f, y_f, z_f) be the coordinates of the arrival point on the surface of an earth-centered sphere of radius R. Let any point on the plane passing through the origin, departure and arrival points be given by (x, y, z). The equation of the plane is obtained by the dot product of a vector defined by the origin and any one of the points on the plane, with a vector normal to the plane. The normal to the plane is obtained by the cross product of vectors defined by the origin and two other points on the plane. This results in the equation of the plane in the form:

$$Ax + By + Cz = 0 \tag{1}$$

with

$$A = y_i z_f - z_i y_f \tag{2}$$
$$B = z_i x_f - x_i z_f \tag{3}$$
$$C = x_i y_f - y_i x_f \tag{4}$$

The coordinates of any point on the sphere of radius R are given in terms of the latitude, λ, and longitude, τ, as:

$$x = R\cos\lambda\cos\tau \tag{5}$$
$$y = R\cos\lambda\sin\tau \tag{6}$$
$$z = R\sin\lambda \tag{7}$$

With these relations, the coordinates of the departure and arrival points are specified in terms of their respective latitudes and longitudes (λ_i, τ_i) and (λ_f, τ_f); thus A, B and C in Equations (2) - (4) are specified constants. Equation of the great circle is obtained by substituting Equations (5) - (7) in the equation of the plane, Equation (1). Thus,

$$\tan\lambda = -\left(\frac{A\cos\tau + B\sin\tau}{C}\right) \tag{8}$$

Great circle distance, l, is obtained by the dot product of the vectors defined by the origin and the departure and arrival points as:

$$l = R\cos^{-1}\left\{\sin\lambda_i\sin\lambda_f + [\cos(\tau_f - \tau_i)]\cos\lambda_i\cos\lambda_f\right\} \tag{9}$$

In the next section the equation of the great circle is used with the equations of motion to derive the heading angle required to fly the great circle route.

3 Navigation Equations

The kinematic equations of motion for a point mass model are given as:

$$\dot{\lambda} = \frac{1}{R}V_g\cos\chi_g \tag{10}$$
$$\dot{\tau} = \frac{1}{R\cos\lambda}V_g\sin\chi_g \tag{11}$$
$$\dot{h} = V_{climb} \tag{12}$$

where, λ is latitude, τ is longitude, h is geometric altitude, R is the mean radius of the Earth, V_g is the

groundspeed, χ_g is the heading angle of the ground-relative velocity vector defined with respect to local north and V_{climb} is the climb rate.

The ground velocity is the resultant of the horizontal components of the airmass-relative velocity and wind velocity, as shown in Figure 1. Magnitude of

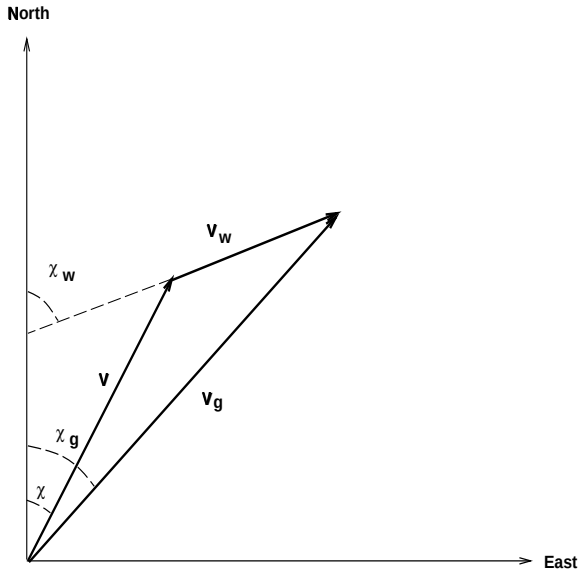

Figure 1: Relative geometry.

the ground velocity vector is called groundspeed, V_g. The magnitude of the horizontal components of the airmass-relative velocity is airspeed, V, and and χ is heading angle of the airmass-relative velocity vector. The magnitude of the horizontal components of the wind velocity W_n and W_e, is windspeed, V_w, where $V_w = \sqrt{W_n^2 + W_e^2}$. Here, W_n, W_e and W_u are the north, east and up components of the wind velocity vector in the local horizontal coordinate frame. The wind heading angle, χ_w, defines the direction of the horizontal component of the wind velocity vector. It is given as: $\chi_w = \tan^{-1}(W_e/W_n)$.

In the aeronautical literature, course angle and track angle are defined as follows. Course angle is associated with the planned path while the track angle is associated with the actual path. In the ensuing discussion it is assumed that the aircraft has a perfect heading control system which maintains track angle equal to the course angle. For heading guidance based on the planned path, χ_g in Equations (10) and (11) is interpreted as course angle. The χ_g that results from the heading χ is interpreted as track angle. To maintain a prescribed course, the aircraft needs to fly a particular heading angle. In the absence of control and wind perturbations, this angle is same as the course angle. However in the presence of wind, the heading angle is offset from the course to compensate for the cross component of wind.

For great circle navigation, the course angle can be determined via Equations (10) and (11) as:

$$\tan\chi_g = \left(\frac{d\tau}{d\lambda}\right)\cos\lambda \tag{13}$$

The derivative of longitude with respect to latitude can be obtained from the equation of the great circle, Equation (8), and substituted into Equation (13) for determination of the following open-loop closed-form solution of the course angle required for flying the great circle route:

$$\chi_g = \tan^{-1}\left\{\frac{C}{\cos\lambda(A\sin\tau - B\cos\tau)}\right\} \tag{14}$$

An alternative navigation law can be developed by using the present aircraft position (λ, τ) and the destination position (λ_f, τ_f) for computation of A, B and C, in Equations (2) - (4). This results in the following closed-loop form:

$$\chi_g = \tan^{-1}\left\{\frac{\sin(\tau_f - \tau)\cos\lambda_f}{\sin\lambda_f\cos\lambda - \sin\lambda\cos\lambda_f\cos(\tau_f - \tau)}\right\} \tag{15}$$

The difference between the two navigation laws, Equations (14) and (15), is that if deviations occur in the first case, the control system is expected to drive the aircraft back to the planned great circle path while in the second case, a new great circle course is set from the present position to destination.

For predicting the location of the airplane between the current time, t_0 and at a future time, t_p, Equation (14) or (15), can be used with Equations (10) and (11) to obtain:

$$\lambda(t_p) = \lambda(t_0) + \frac{1}{R}\int_{t_0}^{t_p} V_g\cos\chi_g dt \tag{16}$$

$$\tau(t_p) = \tau(t_0) + \frac{1}{R}\int_{t_0}^{t_p} \frac{V_g\sin\chi_g}{\cos\lambda} dt \tag{17}$$

Assuming the climb rate to be zero,

$$h(t_p) = h(t_0) \tag{18}$$

Equations (16) and (17) require an estimate of V_g. Following Figure 1 [5],

$$V_g = V\cos\chi_c + V_w\cos\chi_{wg} \tag{19}$$

where, from the law of sines,

$$\chi_c = \sin^{-1}\left(\frac{V_w\sin\chi_{wg}}{V}\right) \tag{20}$$

and

$$\chi_c = \chi_g - \chi \tag{21}$$

$$\chi_{wg} = \chi_w - \chi_g \tag{22}$$

Here, χ_c is the wind correction or crab angle and χ_{wg} is the track-relative wind heading. From Equations (19)

and (20), the groundspeed and the heading angle required for maintaining the course angle of χ_g in a wind field are given as:

$$V_g = V\cos\left\{\sin^{-1}[(\frac{V_w}{V})\sin\chi_{wg}]\right\} + V_w\cos\chi_{wg} \quad (23)$$

and

$$\chi = \chi_g - \sin^{-1}\left\{\frac{V_w}{V}\sin\chi_{wg}\right\} \quad (24)$$

The second term in Equation (24) is the wind correction term. It may be seen that with the heading angle so prescribed, the groundspeed in Equation (23) is only a function of the airspeed, V.

The airspeed, V, in Equation (23) is given in terms of the Mach number, M, and the speed of sound, a, as:

$$V = Ma \quad (25)$$

The speed of sound depends on the absolute temperature, Θ:

$$a = \sqrt{\gamma_{air}R_{air}\Theta} \quad (26)$$

where, γ_{air} is the ratio of specific heats with a value of 1.4 for air, R_{air} is the gas constant with a value of 287.04 J/Kg K [6]. Θ is the absolute temperature measured in degrees Kelvin. The resulting speed of sound is in m/s. With these equations it is seen that either Mach number or airspeed can be used in the groundspeed equation.

Having related the groundspeed to windspeed, wind heading and temperature, it is seen from Equations (16) and (17) that trajectory prediction is possible if these quantities are known. Fortunately, wind and temperature forecasts are provided by the National Oceanic and Atmospheric Administration (NOAA). The NOAA model is described in the Appendix. In the next section the sensitivity of the groundspeed with respect to temperature, wind velocity and wind heading are explored.

4 Groundspeed Sensitivity

Groundspeed sensitivity is defined as the change in groundspeed due to the changes in airspeed, windspeed and track-relative wind heading. Equation (23) shows the dependence of groundspeed on these variables. If Mach number is flown instead of airspeed, Mach number and temperature become independent variables and airspeed becomes a dependent variable via Equations (25) and (26). Clearly, if either Mach or airspeed is controlled directly by a control system, sensitivity with respect them is of little use because the control system is expected to eliminate deviations from the nominal. Thus, either Mach or airspeed can be assumed to be known.

To develop some insight into how windspeed and track-relative wind heading effect the groundspeed, consider the special cases of tailwind, headwind and crosswind. In the tailwind case, $\chi_{wg} = 0$, which leads to:

$$V_g = V + V_w \quad (27)$$

In the headwind case, $\chi_{wg} = \pi$, which results in:

$$V_g = V - V_w \quad (28)$$

In the crosswind case, $\chi_{wg} = \pm\pi/2$, which leads to:

$$V_g = \sqrt{V^2 - V_w^2} \quad (29)$$

These three cases show that windspeed magnitude in the crosswind case has the least impact on the groundspeed. Typically, winds aloft are less than 100 knots, and the aircraft en-route airspeed is about 500 knots. For a windspeed of 100 knots and an airspeed of 500 knots, $V_g = 600$ knots for the tailwind case, $V_g = 400$ knots for the headwind case and $V_g = 490$ knots for the crosswind case. It may be noted that for V_g to change from 600 knots to 400 knots as the track-relative wind heading changes from zero to 180 degrees, V_g has to equal 500 knots at some angle. Thus, groundspeed equals the airspeed at some track-relative wind heading, even for a non-zero wind magnitude.

The sensitivity of groundspeed with respect to airspeed is obtained via Equations (19) and (20) as:

$$\frac{\partial V_g}{\partial V} = \frac{V}{\sqrt{V^2 - V_w^2\sin^2\chi_{wg}}} \quad (30)$$

Using Equations (30), (25) and (26), the sensitivity of groundspeed with respect to temperature can be obtained in terms of the Mach number, temperature and wind terms as:

$$\frac{\partial V_g}{\partial\Theta} = \left(\frac{1.9438M}{2}\right)\sqrt{\frac{\gamma_{air}R_{air}}{\Theta}} \left(\frac{1}{\sqrt{1-\left(\frac{V_w\sin\chi_{wg}}{1.9438M\sqrt{\gamma_{air}R_{air}\Theta}}\right)^2}}\right) \quad (31)$$

Here, R_{air} has units of J Kg/K, Θ has units of K and 1.9438 is the conversion factor from meter/second to knots. This equation is used for generating Figure 2. The Figure shows three graphs corresponding to the no wind case, and 50 knot and 100 knot cases. In each case, the track-relative heading was assumed to be 90 degrees. Thus, these cases represent the worst case scenario as may be verified by inspection of Equation (31). To bring the range of temperatures, shown on the abscissa, in perspective, temperatures of 256 Kelvin and 217 Kelvin correspond to altitudes of 16,000 feet and

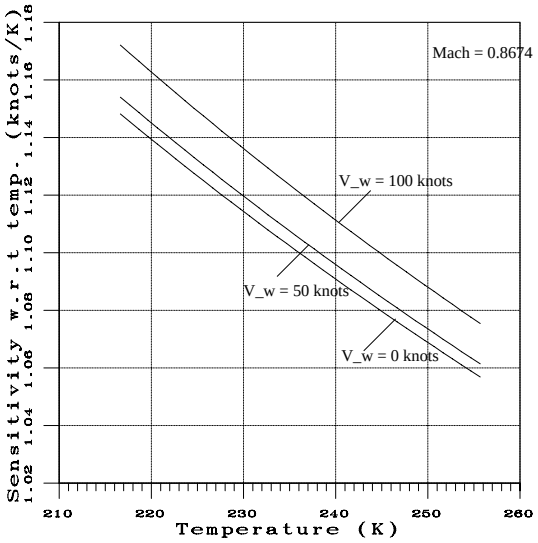

Figure 2: Groundspeed sensitivity with respect to temperature.

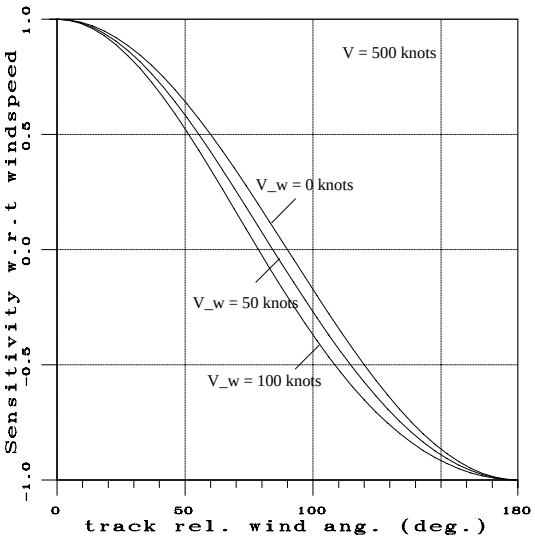

Figure 3: Groundspeed sensitivity with respect to windspeed.

65000 feet in the Standard Atmosphere. The temperature is constant between 36089 feet and 65617 feet altitudes in the 1962 U. S. Standard Atmosphere. Thus, it can be seen from Figure 2, that although there is a slight increase in sensitivity with decreasing temperature or increasing altitude, a nominal value of 1.1 knot per Kelvin can be used.

The sensitivity of groundspeed with respect to windspeed is obtained using Equations (19) and (20) as follows:

$$\frac{\partial V_g}{\partial V_w} = -\frac{V_w \sin^2 \chi_{wg}}{\sqrt{V^2 - V_w^2 \sin^2 \chi_{wg}}} + \cos \chi_{wg} \qquad (32)$$

Figure 3 shows the groundspeed sensitivity with respect to windspeed. The figure illustrates that groundspeed is most sensitive to the windspeed in headwind and tailwind cases. The sensitivity decreases to a minimum of zero somewhere close to 90 degrees. These curves also show that most of contribution to groundspeed sensitivity as a function of airspeed is due to the $\cos \chi_{wg}$ term in Equation (32). The first term in this equation causes a small change in the value of track-relative wind heading at which zero sensitivity occurs.

Finally, the sensitivity of groundspeed with track-relative wind heading is obtained from Equations (19) and (20) as:

$$\frac{\partial V_g}{\partial \chi_{wg}} = -V_w \sin \chi_{wg} \left[\frac{V_w \cos \chi_{wg}}{\sqrt{V^2 - V_w^2 \sin^2 \chi_{wg}}} + 1 \right] \qquad (33)$$

Groundspeed sensitivity as a function of the track-relative wind heading is shown in Figure 4. The curves in this figure illustrate that groundspeed sensitivity

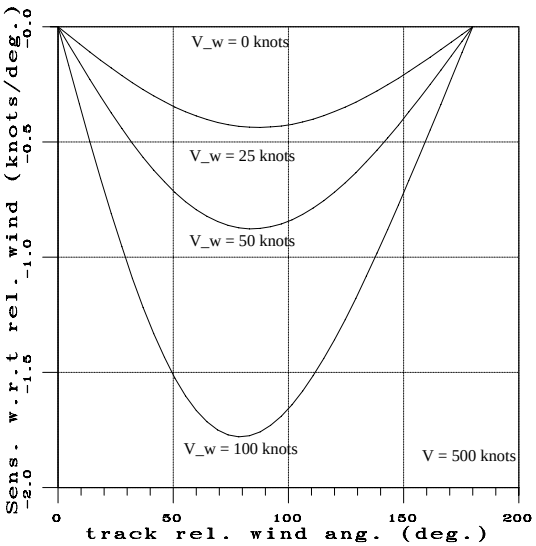

Figure 4: Groundspeed sensitivity with respect to track relative wind heading.

with respect to track-relative wind heading has the maximum magnitude for crosswind. Sensitivity is zero for tailwind and headwind.

In summary, the sensitivity studies indicate the following. For a fixed Mach number, groundspeed sensitivity with respect to temperature increases with decreasing temperature. Groundspeed sensitivity with respect to windspeed is minimum for crosswind and maximum for tailwind and crosswind. Groundspeed sensitivity with respect to track-relative wind heading on the other hand shows an exactly opposite trend. It is maximum for crosswind and minimum for tailwind and headwind.

Since the sensitivity equations also describe the behavior in the neighborhood of the nominal, a linear error model of groundspeed can be developed by using the Taylor Series expansion as:

$$\Delta V_g = \frac{\partial V_g}{\partial \Theta}\Delta\Theta + \frac{\partial V_g}{\partial V_w}\Delta V_w + \frac{\partial V_g}{\partial \chi_{wg}}\Delta(\chi_w - \chi_g) \quad (34)$$

where the Δ quantities represent the respective errors in forecast temperature, windspeed and track-relative wind heading. The partial derivatives are computed at the nominal values of temperature: $\underline{\Theta}$, windspeed: $\underline{V_w}$, and track-relative wind heading: $\underline{\chi_{wg}}$. The partial derivatives are described in Equations (31), (32) and (33). Since the aircraft's heading control system is expected to maintain the ground track, $\Delta\chi_g \approx 0$. Since the primary focus of the present study is trajectory prediction in the presence of winds, temperature dependence is ignored for now. With these assumptions, the error in groundspeed estimate is given as:

$$\Delta V_g = \frac{\partial V_g}{\partial V_w}\Delta V_w + \frac{\partial V_g}{\partial \chi_{wg}}\Delta\chi_w \quad (35)$$

If the nominal values are interpreted as mean values, this equation relates the deviations about the mean. Thus, uncertainty in groundspeed can be predicted based on uncertainty in wind. Eventually, the uncertainty in groundspeed can be propagated into an uncertainty in position. These notions are explored at length in the next section.

5 Trajectory Prediction

The accuracy of trajectory prediction depends on the accuracy of forecasts, on-board equipment used and piloting strategy. For example, in the case where constant airspeed is flown, the predicted groundspeed is not a function of temperature forecast rather, it depends on airspeed measurement accuracy. On the other hand, if a constant Mach is flown, the predicted groundspeed depends on temperature forecast and on the accuracy of Mach measurement. It may be noted that on-board Mach calculations are based on the static and stagnation pressures sensed. If a Flight Management System (FMS) is used with an input cost index for flying great circle segments between waypoints such that the time of arrival at the destination waypoints is fixed, a more precise trajectory estimation may be possible by inclusion of the FMS model in the prediction system. In this research it is assumed that the aircraft is flown with airspeed or Mach number as controls. In the present formulation, the control quantities are not required to be constants but need to be prescribed for the prediction interval. If these quantities are not available, a constant Mach or airspeed assumption can be used.

Given nominal windspeed and wind heading along the great circle, the nominal location of the aircraft can be predicted under the assumption that the aircraft maintains the ground track. The nominal location prediction procedure is described in Table 1.

Table 1: Nominal Trajectory Prediction

1. Set the predicted position to the current position:
   $\underline{\lambda} = \lambda; \quad \underline{\tau} = \tau; \quad \underline{h} = h.$
2. Set time: $t = t_0$.
3. Determine $\underline{W_n}(\underline{\lambda}, \underline{\tau}, \underline{h})$, $\underline{W_e}(\underline{\lambda}, \underline{\tau}, \underline{h})$ from the NOAA wind model data.
4. Compute:
   $\underline{V_w} = \sqrt{\underline{W_n}^2 + \underline{W_e}^2}$
   $\underline{\chi_w} = \tan^{-1}(\underline{W_e}/\underline{W_n})$.
5. Compute $\underline{\chi_g}$ using either Equation (14) or Equation (15) with $\underline{\lambda}$ and $\underline{\tau}$.
6. Compute $\underline{V_g}$ using Equation (23) with $\underline{V}$, $\underline{V_w}$, $\underline{\chi_w}$ and $\underline{\chi_g}$. If Mach is being flown, use $\underline{M}$ and $\underline{\Theta}$ along with Equations (26) and (25) to compute $\underline{V}$.
7. Integrate Equations (10), (11) and (12) as follows:
   $\underline{\tau} = \underline{\tau} + \left(\frac{1}{R\cos\underline{\lambda}}\right)\underline{V_g}\sin\underline{\chi_g}\,\Delta t$
   $\underline{\lambda} = \underline{\lambda} + \left(\frac{1}{R}\right)\underline{V_g}\cos\underline{\chi_g}\Delta t$
   $\underline{h} = \underline{h}$
   to obtain the predicted position at the next time epoch. Δt is the integration step size.
8. Increment time: $t = t + \Delta t$.
9. Stop if $t \geq t_p$; else go to step 3. Note, t_p is the time at which prediction is desired.

Here, t_p is the time at which prediction is desired and Δt is the integration step size.

Since the standard deviations of W_n and W_e provided by NOAA model are known to be between seven to ten knots [9], the uncertainty in position about the nominal can be approximately determined. Consider a variable z which is a function of two random variables x and y. By Taylor Series expansion:

$$z = g(x,y) = g(\underline{x},\underline{y}) + \frac{\partial g}{\partial x}(x-\underline{x}) + \frac{\partial g}{\partial y}(y-\underline{y}) + \cdots \quad (36)$$

Retaining just the first order terms, the variance of z is approximately given as [10]:

$$\sigma_z^2 \approx \left(\frac{\partial g}{\partial x}\right)^2 \sigma_x^2 + \left(\frac{\partial g}{\partial y}\right)^2 \sigma_y^2 + 2\left(\frac{\partial g}{\partial x}\frac{\partial g}{\partial y}\right)\sigma_{xy} \quad (37)$$

Clearly, this approximation is only valid near the means: $\underline{x}$ and $\underline{y}$. Furthermore, this approximation assumes that the function $g(x,y)$ is smooth. In Equation (37), σ_x^2, σ_y^2 and σ_z^2 are the variances of x, y and z; and σ_{xy} is the covariance of x and y. If the two random variables x and y are independent, they are uncorrelated. Thus, the covariance of x and y: $\sigma_{xy} = 0$. This leads to the elimination of the third term in Equation (37).

Using Equation (37) and the definitions of V_w and χ_w:

$$V_w = (W_n^2 + W_e^2)^{\frac{1}{2}} \quad (38)$$

$$\chi_w = \tan^{-1}\left(\frac{W_e}{W_n}\right) \quad (39)$$

the variances of V_w and χ_w can be written as:

$$\sigma_{V_w}^2 \approx \left(\frac{\underline{W_n^2}}{\underline{W_n^2} + \underline{W_e^2}}\right)\sigma_{W_n}^2 + \left(\frac{\underline{W_e^2}}{\underline{W_n^2} + \underline{W_e^2}}\right)\sigma_{W_e}^2 \quad (40)$$

and

$$\sigma_{\chi_w}^2 \approx \left(\frac{\underline{W_e^2}}{(\underline{W_n^2} + \underline{W_e^2})^2}\right)\sigma_{W_n}^2 + \left(\frac{\underline{W_n^2}}{(\underline{W_n^2} + \underline{W_e^2})^2}\right)\sigma_{W_e}^2 \quad (41)$$

In the development of the above relationships, W_n and W_e are assumed to be independent random variables. Furthermore, if the variances of the wind components are assumed to be equal, that is:

$$\sigma = \sigma_{W_n} = \sigma_{W_e} \quad (42)$$

then,

$$\sigma_{V_w}^2 \approx \sigma^2 \quad (43)$$

$$\sigma_{\chi_w}^2 \approx \frac{\sigma^2}{\underline{W_n^2} + \underline{W_e^2}} \approx \frac{\sigma^2}{\underline{V_w^2}} \quad (44)$$

Next, the variance of groundspeed: $\sigma_{V_g}^2$ can be approximated in terms of the variances of windspeed: $\sigma_{V_w}^2$ and wind heading: $\sigma_{\chi_w}^2$ as follows:

$$\sigma_{V_g}^2 \approx \left(\frac{\partial V_g}{\partial V_w}\right)^2 \sigma_{V_w}^2 + \left(\frac{\partial V_g}{\partial \chi_w}\right)^2 \sigma_{\chi_w}^2 \quad (45)$$

The partial derivatives can be evaluated at the nominal values by using Equations (32) and (33). By using Equations (19) and (20) it may be verified that the partial derivative of V_g with respect to χ_w is same as that with respect to χ_{wg}. Since V_w and χ_w are independent and uncorrelated, $\sigma_{V_w\chi_w} = 0$. With the assumptions of Equation (42), a simplified expression for the groundspeed variance can be obtained as:

$$\sigma_{V_g}^2 \approx \left(\frac{\underline{V}^2}{\underline{V}^2 - \underline{V_w^2}\sin^2\underline{\chi_{wg}}}\right)\sigma^2 \quad (46)$$

Closer examination of this expression shows that $\sigma_{V_g}^2 \approx \sigma^2$. Clearly this is true for the headwind and tailwind cases. Note that $\sigma_{V_g}^2$ is maximum for the pure crosswind case. Also, $\sigma_{V_g}^2$ increases with increasing V_w. As an example, consider the case of a 100 knot crosswind. If the airspeed is assumed to be 500 knots, $\sigma_{V_g}^2 = 1.04\sigma^2$. This example shows that $\sigma_{V_g}^2 \approx \sigma^2$ is a good approximation irrespective of the track-relative wind heading.

Finally, the uncertainty in the groundspeed translates into an uncertainty in the aircraft position given by the latitude and longitude. The latitude and longitude uncertainty can be obtained by integrating the navigation Equations (10) and (11). However, it may be observed that the latitude Equation (10) is independent of longitude while the longitude Equation (11) depends on the latitude. Since the latitude and longitude are related to each other along the great circle route via Equation (8), this equation can be used for obtaining the following navigation equation:

$$\dot{\lambda} = \left\{\frac{A\sin\tau - B\cos\tau}{RC}\right\} V_g \cos\lambda \sin\chi_g \quad (47)$$

Equation (11) forms the other navigation equation. Note that with λ and τ as the two states, Equations (47) and (11) form the state equations.

Linearizing Equations (47) and (11) about the nominal great circle trajectory, the following state equation is obtained.

$$\begin{bmatrix} \delta\dot{\lambda} \\ \delta\dot{\tau} \end{bmatrix} = \begin{bmatrix} F_{11} & F_{12} \\ F_{21} & F_{22} \end{bmatrix} \begin{bmatrix} \delta\lambda \\ \delta\tau \end{bmatrix} + \begin{bmatrix} G_1 \\ G_2 \end{bmatrix} \delta V_g \quad (48)$$

where,

$$F_{11} = -\left\{\frac{A\sin\underline{\tau} - B\cos\underline{\tau}}{RC}\right\}\underline{V_g}\sin\underline{\lambda}\sin\underline{\chi_g} \quad (49)$$

$$F_{12} = \left\{\frac{A\cos\underline{\tau} + B\sin\underline{\tau}}{RC}\right\}\underline{V_g}\cos\underline{\lambda}\sin\underline{\chi_g} \quad (50)$$

$$F_{21} = \left\{\frac{\tan\underline{\lambda}}{R\cos\underline{\lambda}}\right\}\underline{V_g}\sin\underline{\chi_g} \quad (51)$$

$$F_{22} = 0 \quad (52)$$

and

$$G_1 = \left\{\frac{A\sin\underline{\tau} - B\sin\underline{\tau}}{RC}\right\}\cos\underline{\lambda}\sin\underline{\chi_g} \quad (53)$$

$$G_2 = \frac{\sin \underline{\chi}_g}{R \cos \underline{\lambda}} \quad (54)$$

Here, δV_g appears as control in the state Equation (48). The underlined quantities in the above equations are the nominal values along the great circle trajectory.

Let $P(t)$ be the state covariance matrix at any time t. Starting with the initial covariance matrix at time t_0, the covariance matrix at the prediction time t_p can be obtained by the following covariance propagation equation [11]:

$$\dot{P}(t) = F(t)P(t) + P(t)F^T(t) + G(t)Q(t)G^T(t) \quad (55)$$

where $F(t)$ is the plant matrix, $G(t)$ is the disturbance distribution matrix and $Q(t)$ is the spectral density matrix. It may be noted that the spectral density matrix may be converted to the covariance matrix by multiplication with the Dirac delta function [11]. The elements of $F(t)$ and $G(t)$ matrices are given in Equations (49) through (54). It may be observed from Equation (48) that in this case, $Q(t)$ is just a scalar corresponding to the spectral density of the groundspeed uncertainty. Initially, the four elements of $P(t)$ can be set to zero. With the various matrices so specified, the state covariance at any time t can be obtained by integrating Equation (55). The steps needed for propagating the covariance matrix to time t_p are summarized in Table 2.

Table 2: Covariance Propagation Summary

1. Compute $\underline{V}_g(t)$, $\underline{\chi}_g(t)$, $\underline{\lambda}(t)$ and $\underline{\tau}(t)$ using the procedure described in Table 1.
2. Set $t = t_0$; $P(t_o) = [0]$ and $Q(t) = Q(t_0) = \sigma^2$ where σ^2 is the variance of the wind velocity components.
3. Compute the elements of the $F(t)$ matrix and $G(t)$ vector using Equations (49) through (54).
4. Integrate Equation (55) with step size Δt to obtain $P(t + \Delta t)$.
5. Increment time: $t = t + \Delta t$.
6. If $t \geq t_p$ stop; else, go to step 3.

The latitude and longitude uncertainties are completely specified by the covariance matrix $P(t)$. Let P_{11}, P_{12}, P_{21} and P_{22} be the elements of the covariance matrix. The principal direction of the covariance matrix θ_p can be computed in terms of its elements as [12]:

$$\theta_p = \left(\frac{1}{2}\right) \tan^{-1}\left[\frac{2P_{12}}{P_{11} - P_{22}}\right] \quad (56)$$

The latitude and longitude are correlated in terms of this angle as follows:

$$\tau = \tan\theta_p(\lambda - \underline{\lambda}) + \underline{\tau} \quad (57)$$

The three times standard deviation bounds of longitude can be obtained by substituting,

$$\lambda = \underline{\lambda} \pm 3\sqrt{(P_{11})} \quad (58)$$

in Equation (57). Clearly, Equation (57) cannot be used if $\theta_p = 90°$. In this case the alternative equation,

$$\lambda = \left(\frac{1}{\tan\theta_p}\right)(\tau - \underline{\tau}) + \underline{\lambda} \quad (59)$$

should be used. In this case, the three times standard deviation bounds of latitude can be obtained by using,

$$\tau = \underline{\tau} \pm 3\sqrt{(P_{22})} \quad (60)$$

in Equation (59).

6 Simulation Results

To demonstrate the prediction accuracy using the methods described in the previous section, the initial 20 minute segment of the great circle trajectory from San Francisco to Boston is considered. The aircraft airspeed of 500 knots, a tailwind of 100 knots with the standard deviation of 10 knots in the north and east components is assumed.

The actual trajectory of the aircraft is simulated at one second intervals by adding white noise with a standard deviation of 10 knots to each wind component. The cross component of the wind is corrected by suitably crabbing with respect to the desired course. The remaining alongtrack component of the wind is added to the alongtrack component of the airspeed to obtain the groundspeed. The navigation Equations (10) and (11) are then integrated to obtain the aircraft position in 20 minutes. The procedure for obtaining the actual position follows the procedure for predicting the nominal position with actual values rather than the nominal values. The procedure for predicting the nominal position was described in Table 1.

The predicted nominal trajectory for 20 minutes is synthesized using the steps described in Table 1. The nominal tailwind of 100 knots and alongtrack airspeed of 500 knots is used for this purpose. The predicted nominal trajectory for 20 minutes is shown in Figure 5.

For covariance propagation, the standard deviation of groundspeed is assumed to be 10 knots. Driven by

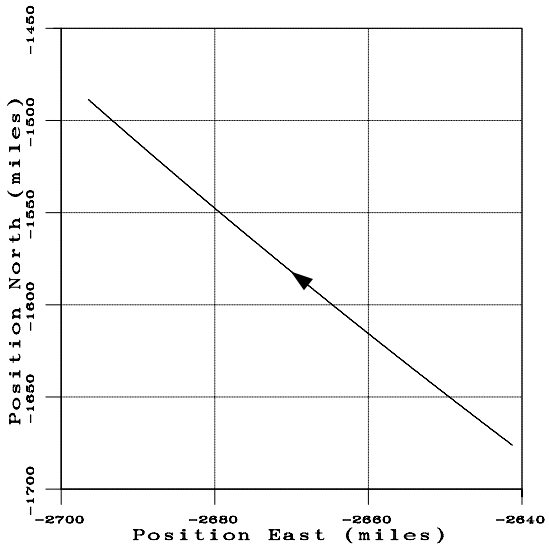

Figure 5: Predicted nominal trajectory.

the groundspeed uncertainty, the covariance matrix is propagated to the prediction time using the procedure described in Table 2. The covariance matrix at the prediction time $P(t_p)$ is then used in Equation (56) through (59) to obtain the uncertainty bounds of latitude and longitude. These uncertainty bounds can be used for determination of the inertial position bounds using Equations (5) through (7). These bounds are shown in Figure 6. Figure 6 also shows the aircraft

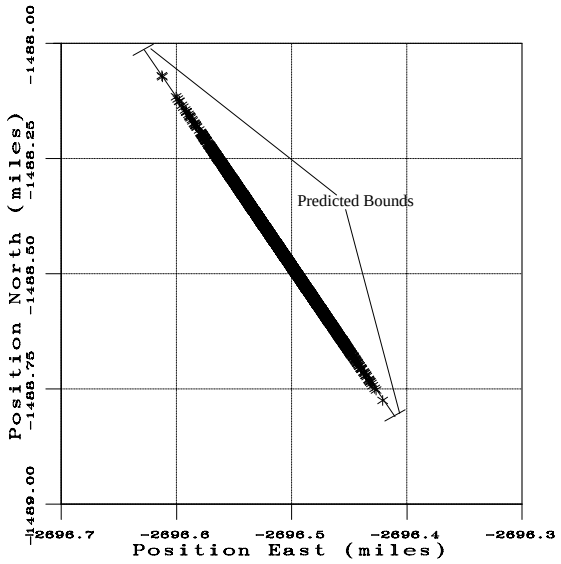

Figure 6: Predicted position bounds.

positions for the 5000 Monte Carlo runs. The actual trajectory for these runs were simulated using the procedure discussed earlier.

Figure 6 shows that the the position uncertainty bounds for the 20 minute prediction interval are quite accurately predicted by the procedures described in this paper.

7 Conclusions

Trajectory prediction into the future during en-route flight requires knowledge of aircraft controls, and forecast wind and temperature. Aircraft controls are assumed to be the heading angle and Mach number or airspeed. Mach number or airspeed are known from flight plans or Air Traffic Control clearances. The heading angle depends on the course angle, windspeed and wind heading. For this purpose, the course angle was obtained in closed-form based on the equation of the great circle. The expression for heading angle was then derived. Thus, one of the controls was eliminated. Next, a wind forecast model that provides the wind and temperature data was described. Since trajectory prediction depends on the estimated groundspeed, its sensitivities with respect to temperature, windspeed and track-relative wind heading were examined. An error model was developed using the sensitivity equations. Subsequently, an algorithm was presented for predicting the nominal trajectory based on the data derived from the forecast model. Finally, an algorithm for estimating error bounds around the nominal trajectory was presented. The error bounds were determined by propagating the wind forecasting errors along the nominal trajectory using the error model. Results obtained via Monte Carlo simulations were used for verification of the error bound determination procedure.

References

[1] Air Traffic Rules and Procedures Service, **Air Traffic Control FAA Order 7110.65**, FAA, U. S. Department of Transportation.

[2] **Report of the RTCA Board of Directors' Select Committee on Free Flight**, Dec. 16, 1994.

[3] Howells, P. J., "Aircraft Trajectory–Prediction and Control in the Air Transport Flight Management Computer Systems," *NATO Advisory Group for Aerospace Research and Development*, AGARD-AG-301, Vol. 1.

[4] Weinstock, R., **Calculus of Variations with Applications to Physics and Engineering**, Dover Publications, Inc., New York, 1974.

[5] Slattery, R. A., "Terminal Area Trajectory Synthesis for Air Traffic Control Automation," *Proc. of the American Control Conf.*, Seattle, WA, 1995.

[6] Saad, M. A., **Compressible Fluid Flow**, Second Edition, Prentice-Hall, Englewood Cliffs, New Jersey 07632, 1993.

[7] Benjamin, S. G., Brewster, K. A., Brümmer, R., Jewett, B. F., Schlatter, T. W., Smith, T. L., and Stamus, P. A., "An Isentropic Three-Hourly Data Assimilation System Using ACARS Aircraft Observations," *Monthly Weather Review*, Vol. 119, April, 1991, pp. 888-906.

[8] Snyder, J. P., **Map Projections Used by the U. S. Geological Survey**, Geological Survey Bulletin 1532, Second Edition, U. S. Government Printing Office, Washington, D. C., 1982.

[9] Dévényi, D., and Schlatter, T. W., "Statistical properties of Three-Hour Prediction "Errors" Derived from the Mesoscale Analysis and Prediction System," *Monthly Weather Review*, Vol. 122, June, 1994, pp. 1263-1280.

[10] Papoulis, A., **Probability, Random Variables, and Stochastic Processes**, McGraw-Hill, Inc., San Francisco, 1965.

[11] Gelb, A., (ed.), **Applied Optimal Estimation**, The M. I. T. Press, Massachusetts Institute of Technology, Cambridge, MA 02142.

[12] Jain, A. K., **Fundamentals of Digital Image Processing** Prentice-Hall, Englewood Cliffs, NJ 07632.

A Wind Forecast Model

Mesoscale Analysis and Prediction System (MAPS) is used by NOAA for providing the horizontal wind components at different levels over the United States, northern Mexico and southern Canada every three hours [7]. MAPS assimilates observations from rawinsondes, surface observations, wind profiler measurements and automated aircraft reports. During the three hour assimilation cycle, vertical and horizontal consistency checks are performed on all observations. Several quality control procedures are described in [7]. Every three hours forecasts are made out to 12 hours using an analysis technique formulated in a hybrid vertical coordinate consisting of terrain-following coordinates close to the ground and isentropic coordinates above them. In the isentropic coordinate system, atmospheric features such as fronts and jet streams, appear with greater coherence [7]. With the hybrid system greater accuracy is achieved close to the ground and in the troposphere.

Forecast from the previous assimilation cycle forms the background for the next three hour assimilation cycle. During the assimilation cycle, the background analysis is subtracted from all observations and the analysis increment is calculated. This increment is then added to the background to generate the final analysis. Since MAPS uses variables which are slightly unconventional, the output is converted to more familiar variables such as isobaric levels between 1000 and 100 hectopascals (hPa), with 25 hPa resolution. Output variables on these surfaces include temperature, geopotential altitudes, relative humidity, and horizontal wind components W_n and W_e. All outputs are reported on the MAPS grid system.

The horizontal resolution of the MAPS grid is 60 km and the grid contains 81 by 62 grid points. A polar stereographic projection which is a special case of stereographic projection, shown in Figure 7, is used for mapping to the MAPS grid. Figure 7 shows how wind

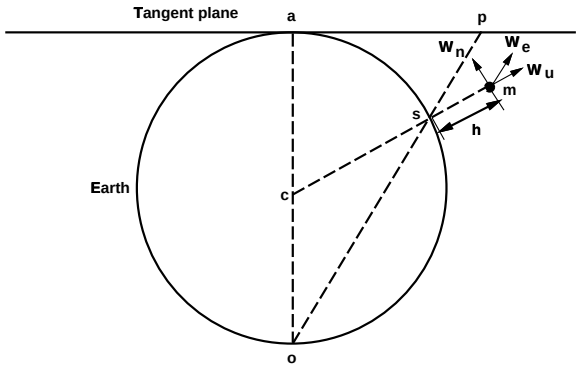

Figure 7: Polar stereographic projection.

velocity components in the local horizontal frame are reported on a tangential plane. Assume that wind velocity vector components in the horizontal plane at **m**, are W_n and W_e. Stereographic projection is accomplished by projecting a line from **o** through **s** to meet the tangent plane at **p**. The north and east components of the wind are reported at **p**. It may be noted that the projection point **o** is located at the opposite pole such that the normal from the tangency point **a** passes through **o**. Point **s** is defined by the intersection of the line **mc** with the surface where **c** is the earth center. From the figure it may be seen that data along line **mc** are projected to the same location on the plane. Thus to report the third coordinate such as pressure or altitude, separate tangent planes are required. To report data at regular pressure or altitude intervals, a regular three dimensional rectangular grid is used in which the two coordinates are associated with the stereographic projection and the third coordinate is the pressure, which can be transformed to altitude.

Given the point of tangency specified in terms of (λ_a, τ_a), the stereographic projection of point **s** onto the tangent plane is [8]:

$$x_p = Rk \cos\lambda_s \sin(\tau_s - \tau_a) \quad (61)$$

$$y_p = Rk[\cos\lambda_a \sin\lambda_s - \sin\lambda_a \cos\lambda_s \cos(\tau_s - \tau_a)] \quad (62)$$

where:

$$k = \frac{2}{[1 + \sin\lambda_a \sin\lambda_s + \cos\lambda_a \cos\lambda_s \cos(\tau_s - \tau_a)]} \tag{63}$$

and (λ_s, τ_s) is the location of point **s**. The special case of north polar stereographic projection, used by NOAA, is obtained by setting λ_a to 90 degrees in the above equations.

Having offered a brief introduction to the wind prediction model, a brief summary of the statistical properties of the prediction errors derived from MAPS is provided next. The research in [9] studied the statistical properties of the residual, defined as the difference between the observed and forecasted values. The dataset for the study was collected over a three month period in 1993. For computation of the statistical quantities, residuals at rawinsonde locations in the United States were used. The study found that the mean values of the residuals in the north and east components of the wind are less than 1 m/s at every isentropic level and at most levels less than 0.3 m/s. Standard deviations of the wind components were found to increase with height in accordance with the normal increase of the zonal wind. Skewness in the each wind component was found to be 0.1 indicating a nearly symmetric distribution and the flatness was found to be usually greater than 4 indicating long tails in the distribution.

For trajectory prediction, standard deviation or variance of the wind components are important because wind estimation errors directly translate into aircraft position estimation errors. The variation of standard deviation reported in [9] as a function of isentropic levels is presented in Figure 8 as a function of pressure altitude based on the Standard Atmosphere. It is noted

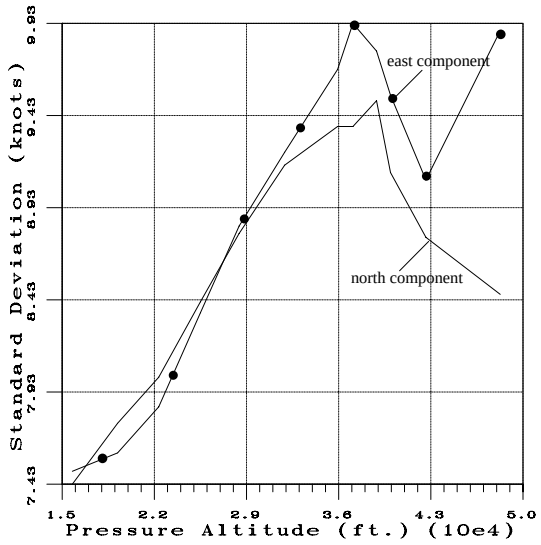

Figure 8: Standard deviations of wind components.

that the standard deviation value at 48000 feet is based on small data samples hence it is unreliable [9]. The graphs show that the standard deviations of the north and east components vary between 7 and 10 knots for the range of altitudes important for en-route flight.